Osmotic properties of T cells determined by flow imaging microscopy in comparison to electrical sensing zone analysis

Roesch, A.; Windisch, R.; Wichmann, C.; Wolkers, W.F.; Kersten, G.; Menzen, T.

Cryobiology 113 (2023) 104587

Contents lists available at ScienceDirect

Cryobiology

journal homepage: www.elsevier.com/locate/cryo

Osmotic properties of T cells determined by flow imaging microscopy in comparison to electrical sensing zone analysis

Alexandra Roesch [a,b], Roland Windisch [c], Christian Wichmann [c], Willem F. Wolkers [d,e], Gideon Kersten [a,b], Tim Menzen [a,*]

[a] Coriolis Pharma, Fraunhoferstr. 18 b, 82152, Martinsried, Germany
[b] Leiden Academic Centre for Drug Research (LACDR), Leiden University, PO Box 9502, 2300, RA, Leiden, the Netherlands
[c] Division of Transfusion Medicine, Cell Therapeutics and Haemostaseology, University Hospital, LMU Munich, Munich, Germany
[d] Unit for Reproductive Medicine – Clinic for Horses, University of Veterinary Medicine Hannover, Hannover, Germany
[e] Biostabilization Laboratory – Lower Saxony Centre for Biomedical Engineering, Implant Research and Development, University of Veterinary Medicine Hannover, Hannover, Germany

ARTICLE INFO

Keywords:
Cryoprotectant loading
Cryoprotective agent
Cell viability
Flow imaging microscopy
Membrane permeability
Osmotic tolerance limit
Cryopreservation

ABSTRACT

To develop cryopreservation methods for cell-based medicinal products it is important to understand osmotic responses of cells upon immersion into solutions with cryoprotective agents (CPAs) and during freezing. The aim of this study was to assess the osmotic response of T cells by using flow imaging microscopy (FIM) as a novel cell-sizing technique, and to corroborate the findings with electrical impedance measurements conducted on a Coulter counter. Jurkat cells were used as a potential model cell line for primary T cells. Cell volume responses were used to derive important cell parameters for cryopreservation such as the osmotically inactive cell volume V_b and the membrane permeability towards water and various CPAs. Unlike Coulter counter measurement, FIM, combined with Trypan blue staining can differentiate between viable and dead cells, which yields a more accurate estimation of V_b. Membrane permeabilities to water, dimethyl sulfoxide (Me_2SO) and glycerol were measured for Jurkat cells at different temperatures. The permeation of Me_2SO into the cells was faster in comparison to glycerol. CPA permeation decreased with decreasing temperature following Arrhenius behavior. Moreover, membrane permeability to water decreased in the presence of CPAs. V_b of Jurkat cells was found to be 49% of the isotonic volume and comparable to that of primary T cells. FIM proved to be a valuable tool to determine the membrane permeability parameters of mammalian cells to water and cryoprotective agents, which in turn can be used to rationally design CPA loading procedures for cryopreservation.

1. Introduction

Cell-based medicinal products (CBMPs) are emerging therapeutics with several approved products on the market, as well as an increasing number entering clinical trials [26]. Being complex and fragile entities CBMPs pose challenges for drug product development including stabilization and storage. In liquid state without cell culture conditions, e.g., during production, handling, administration and short-term storage, cells typically survive only for 1–4 days depending on the cell type and storage temperature (refrigerated or room temperature) [1,13]. Therefore, CBMPs are usually stored at temperatures below −120 °C for long-term storage and transportation [11]. Maintaining the biological activity of CBMPs upon storage and transportation in frozen state is essential and several factors, such as the cooling rate, the cell concentration or sample volume, may affect cryopreservation quality [3,4]. To enable high viability after thawing, cryoprotective agents (CPAs) such as dimethyl sulfoxide (Me_2SO) or glycerol are commonly used in concentrations of 0.5–3 M [4]. Both molecules pass the cell membrane and protect the cells by preventing intracellular ice formation as well as reducing solute damage [7,17]. Additionally, disaccharides, e.g., sucrose or trehalose can be used as non-permeating CPAs to protect cell membrane proteins and cell membranes [4], and to increase the glass transition temperature of the freeze-concentrated formulation [24]. A better understanding of the osmotic response of cells aids in development of rationally designed protocols for successful cryopreservation of CBMPs. Key parameters are the osmotically inactive cell volume (V_b) as

* Corresponding author.
E-mail address: Tim.Menzen@coriolis-pharma.com (T. Menzen).

https://doi.org/10.1016/j.cryobiol.2023.104587
Received 21 July 2023; Received in revised form 20 September 2023; Accepted 24 September 2023
Available online 1 October 2023

well as cell membrane permeability to water (L_p) and CPA (P_s) [8]. CPA loading is a critical process step during cryopreservation because cell volume excursions due to the osmotic pressure have to remain within the tolerance limits of the cells [12]. Also, a sufficiently long equilibration time between adding the cryoprotectants and starting the freezing has to be chosen to ensure permeation of the CPA into the cell [12]. Upon addition of a CPA solution, water moves out of the cell due to the osmotic pressure followed by CPA penetration into the cell in case of Me_2SO or glycerol. Based on the detected volume change (shrink – swell process) L_p and P_s can be calculated [14].

Chimeric antigen receptor (CAR) T cell therapy products are a prominent class of CBMPs, which enable the treatment of various severe cancer diseases [26]. To produce CAR T therapy products, human T cells are isolated from the patient, shipped to a manufacturing site in which they are transduced with a CAR gene construct, expanded, washed, formulated (i.e., cryopreserved) and returned to the clinic for infusion into the patient [2]. Because donated T cells as well as the final CAR T cell therapy product are scarce and expensive, model cells are used. Particularly Jurkat cells, an immortalized human T cell line, are frequently used as model for T cells [9,10,20].

The osmotic response of cells, i.e., the process of cell swelling or shrinking upon exposure to hypotonic or hypertonic solutes is commonly studied with microscopic set-ups [8,25,30] or with the electrical sensing zone/Coulter principle [5,27]. Both options have their limitations and drawbacks, e.g., a limited number of investigated cells (microscopy) and the inability to discriminate viable cells from dead cells and other particulate impurities of the same size (Coulter counter). To circumvent those drawbacks, in this work new methods based on flow imaging microscopy (FIM) were established to determine osmotic parameters of Jurkat and primary T cells. Using a microscopic flow-cell setup, FIM instruments provide bright-field images of a large number of cells per measurement and are commonly used for sizing and characterization of particles in the micrometer size range [31]. In this work, FIM was used to differentiate viable cells from dead cells and cell debris based on the observed morphology and the osmotic response was determined for viable cells obtained from the change in the calculated cell volume. In particular, Me_2SO and glycerol were used as permeable CPAs, whereas sucrose was chosen as an impermeable CPA. Membrane permeabilities were determined from cell volume upon exposing the cells to CPA solutions or anisotonic media by fitting the data with the 2P formalism [14]. Cell volume responses were recorded at different temperatures to determine activation energies of water and CPA transport across the cell membranes.

2. Material & methods

2.1. Jurkat cells cultivation and T cell isolation

The immortalized T cell line Jurkat (clone E6.1) was purchased from CLS GmbH (Eppelheim Germany) and cultured in Roswell Park Memorial Institute (RPMI) 1640 medium (Thermo Fisher Scientific) supplemented with 10% fetal calf serum (FCS) (Bio&Sell GmbH) at a density between 0.5×10^6–3×10^6 cells ml^{-1}. Cells were freshly harvested prior experimental work by centrifugation at 400*g* and resuspended in fresh RPMI medium. Cells were diluted to a concentration of 1×10^6 cells ml^{-1} as starting material.

Peripheral blood mononuclear cells (PBMC) were purchased from PeloBiotech (Planegg, Germany). PBMC were stored frozen at −145 °C before use. T cells were isolated by using the Pan T cell isolation kit, human obtained from Miltenyi Biotec (Bergisch Gladbach, Germany) according to the manufacturer's instruction. In short, PBMC were thawed at 37 °C in a water bath, centrifuged at 400 g for 8 min and resuspended in phosphate buffered saline (PBS; Gibco, pH 7.4) supplemented with 0.5% bovine serum albumin (BSA) and 2 mM EDTA. All non T cells were labelled by adding Pan T cell Biotin-Antibody cocktail to the PMBC suspension and incubated for 5 min in the refrigerator (2–8 °C). In the following Pan T cell Microbead Cocktail was added and incubated for 10 min in the refrigerator. Subsequently, T cells were manually separated in the magnetic field of a MACS separator. Isolated T cells were directly used for experiments within 5 h after initial cell thawing.

PBS and Trypan blue solution 0.4% (Gibco) were obtained by ThermoFisher. Fluorescent dyes Calcein AM and Dead Cell Apoptosis Kit containing AnnexinV, fluorescein isothiocyanate (FITC) and propidium iodide (PI) were also obtained from ThermoFisher. Sucrose, dimethyl sulfoxide and glycerol were purchased from Sigma Aldrich.

2.2. Cell volume determination by flow imaging microscopy (FIM)

Cell volumes were determined by FIM using a FlowCam 8100 (Fluid Imaging Technologies, Scarborough, USA). A 10× magnification objective was used and particles were captured by a high-resolution CMOS camera (1920 × 1200 pixels) at 34 frames per second. The intensity thresholds, which pixel difference compared to the background defines a particle, were 17 for dark pixels and 15 for light pixels. In between measurements the flow cell was thoroughly flushed with 1% (w/v) Terga-a-zyme enzyme detergent and highly purified water. Jurkat cells as well as primary human T cells were analyzed. As described below, the cell volume was measured after equilibration in osmotic solutions as well as kinetic measurements directly upon addition to osmotic solutions. To all cell samples measured with FIM Trypan blue solution was added to stain dead cells. Osmotically equilibrated experiments were performed with a flow rate of 0.2 ml min^{-1} over a measurement time of 2 min and the sample volume was 500 µl. Three replicates were measured on different measurement days. To measure the kinetic volume change of cells several adaptions were made to the instrumental set-up (Fig. S1). In short, the upper tubing of the instrument's original sample holder was removed and an alternative sample port was built based on a 25-ml Combitip generating a broader sample funnel and shortening the dead-volume until the flow cell. Consequently, the time lag until the first cell image is obtained is dramatically reduced to ca. 8–10 s after starting the measurement. First, osmotic solutions were pipetted into the sampling funnel and upon cell addition the measurement was directly started. A homogenous cell suspension was achieved by pipetting the liquid in the funnel up and down. Based on the visual distribution of Trypan blue in the funnel, the cells and the osmotic solution were completely mixed within 3–4 s. The flow rate was kept at 0.2 ml min^{-1}, whereas the sampling volume was 1 ml and the measurement time 5 min. A cell volume measurement in PBS was performed to determine isotonic cell volume at the beginning of each measurement day. Cell volumes were derived from the instrument's software (VisualSpreadsheet version 4).

2.3. Cell volume determination of Jurkat cells by Coulter counter

Experiments were performed with a Coulter counter Multisizer 4 (Beckman Coulter) using a 100-µm aperture tube. Similar to FlowCam measurements static measurements as well as time resolved measurements were performed with Jurkat cells. For static measurements the Beckman Coulter sampling vials were used and three replicates were measured. Time resolved measurements were performed in a 100-ml beaker including the built-in stirrer option. Cells were added into the beaker pre-filled with the respective osmotic solution and the measurement was directly started. To evaluate the mixing of cells and solution Trypan blue dye was used and a homogeneous staining was observed within approximately 3 s. Prior to each measurement the osmotic solution was replaced and the system was calibrated using 10-µm latex beads (Beckman Coulter). Cell volume was derived from the instrument's software (Multisizer 4.01). Similar to FIM a measurement of cell volume in PBS was performed to determine isotonic cell volume at the beginning of each measurement day as also the Coulter counter has a small time lag of ca. 8 s until the first cells are measured.

2.4. Osmotically inactive cell volume derived from Boyle van't Hoff plot

Osmotic solutions were prepared by adding 50–150 mM sucrose to PBS resulting in tonicities of 350, 400, 420 and 450 mOsm kg^{-1}. PBS was used as isotonic solution (M_0). To determine the osmotically inactive cell volume, cells were incubated in different osmotic solution for 5 min prior to measurements. By dividing the cell volume by the volume in isotonic solution the normalized cell volume V_n was calculated. Boyle van't Hoff plots were generated by plotting V_n against the reciprocal of the external medium osmolality divided by the isotonic osmolality ($\frac{M_0}{M}$). The normalized cell volume V_n can be described using the following equation:

$$V_n = (1 - V_b) \times \left[\frac{M_0}{M}\right] + V_b.$$

An overview of the described parameters and their units is provided in Table 1. The osmotically inactive cell volume V_b can be derived from the y-intercept, i.e., the normalized cell volume at infinite osmolality [16]. Jurkat cells were measured with FIM and Coulter counter, whereas T cells were only measured with FIM. Viable cells were selected by using morphological filter applied to the particle images obtained by FIM. Several morphological parameters provided by the instrument's software were used to differentiate between viable and dead cells: "Pixel intensity" was used to differentiate Trypan blue stained dead cells from viable cells. Additionally, "aspect ratio", "circle fit" and "symmetry" were used to remove aggregated cells or cell debris. A size filter based on the cell's diameter was also applied. Furthermore, "sigma intensity" and "edge gradient" were used to remove out-of-focus cells. The remaining cells were considered as viable cells. For Coulter counter measurements all cells within the same diameter range as used for FIM (6–22 μm) were used to calculate the average cell volume per osmotic solution. Detailed settings of the mentioned morphological parameters which were used for both cell types are provided in Tables S1 and S2.

2.5. Membrane permeability of cells towards water and cryoprotective agents

Cell membrane permeability was determined by time resolved measurements upon addition of cells to different CPAs. The two-parameter transport formalism was used to derive L_p and P_s [14]:

$$\frac{dVw}{dt} = -L_P \times A \times R \times T \times \left[M^e - M^i\right],$$

Table 1
Overview of parameters and their unit in the order of appearance in the text.

Parameter	Description	Unit
V	cell volume	μm^3
V_n	normalized cell volume	relative unit
M_0	isotonic osmolality	mOsm kg^{-1}
M	external medium osmolality	mOsm kg^{-1}
V_b	osmotically inactive cell volume	relative unit
L_p	cell membrane permeability towards water	μm min^{-1} atm^{-1}
P_s	cell membrane permeability towards CPA	μm min^{-1}
A	cell area	μm^2
R	ideal gas constant	μm^3 atm K^{-1} mol^{-1}
T	temperature	Kelvin (K)
M^e	medium osmolality	mol μm^{-3}
M^i	internal osmolality	mol μm^{-3}
$\overline{V_s}$	partial molar volume of permeating solute	μm^3 min^{-1}
E_{Lp}	activation energy for water transport	kcal mol^{-1}
E_{Ps}	activation energy for CPA transport	kcal mol^{-1}
$L_{p,ref}$	cell membrane permeability towards water at reference temperature T_{ref}	μm min^{-1} atm^{-1}
$P_{s,ref}$	cell membrane permeability towards CPA at reference temperature T_{ref}	μm min^{-1}

$$\frac{dVs}{dt} = P_S \times A \times \left[M_s^e - M_s^i\right] \times \overline{V_s},$$

where V_W is the water volume, V_s the solute volume, A refers to the cell area, T to the temperature and R is the ideal gas constant, which equals 8.206×10^{13} μm^3 atm K^{-1} mol^{-1} (Table 1). Osmolalities are described by M^e for medium osmolality, M^i for internal cell osmolality, M_s^e refers to the extracellular permeating solute osmolality and M_s^i to the intracellular permeating solute osmolality. Partial molar volume of the permeating solute is described by $\overline{V_s}$. The equations were used to fit cell volume versus time plots with the software MATLAB. As osmotic solutions sucrose in PBS (osmolality: 450 mOsm kg^{-1}), 1.4 M Me_2SO in PBS as well as 1.4 M glycerol in PBS were used. Membrane permeability was determined with FIM for Jurkat cells and primary T cells and with Coulter counter for Jurkat cells. Cell volume was normalized using the isotonic cell volume measured for each day (=starting volume). A Gaussian filter, i.e., gaussian-weighted average over 1500 datapoints, was applied to smooth the data points. Tables S3 and S4 provide morphological parameters used for kinetic measurements for Jurkat and primary T cells. Membrane permeability was measured at different temperatures for Jurkat cells, where each solution was precooled, i.e., on ice or in a refrigerator, or prewarmed in a water bath. The actual temperature of each sample was measured at the beginning of the measurement.

2.6. Activation energy of transport processes of Jurkat cells

To determine the temperature dependence of L_p and P_s for Jurkat cells an Arrhenius plot was generated based upon [27]:

$$\ln(L_p) = \ln(L_{p,ref}) - \left(\frac{E_{Lp}}{R}\right) \times \left(\frac{1}{T} - \frac{1}{T_{ref}}\right),$$

$$\ln(P_s) = \ln(P_{s,ref}) - \left(\frac{E_{Ps}}{R}\right) \times \left(\frac{1}{T} - \frac{1}{T_{ref}}\right),$$

where E_{Lp} and E_{Ps} represent the activation energies (in kcal mol^{-1}) for water and CPA transport across cell membrane, respectively (Table 1).

2.7. Cell viability determination with imaging flow cytometry

To determine cell viability two different fluorescence assays were used and measured with imaging flow cytometry using an Amnis FlowSight instrument (Luminex) and data were analyzed with the software IDEAS 6.2.183 (Luminex). Calcein AM and propidium iodide dye were used to stain viable and dead cells, respectively. Additionally, AnnexinV-FITC and PI were used to stain apoptotic and dead cells, respectively. Each measurement was performed in duplicate.

3. Results

3.1. Determination of cell viability with flow imaging microscopy

FIM provides bright-field images of the cells that are captured by camera in the flow cell. During one measurement of 0.27 ml, approximately 30,000–80,000 particles in a size range of 1–100 μm were detected (Tables S5 and S6). During data analysis with the instrument's software, morphological filters (Tables S1 and S2) are used to classify the particle images. Based on the morphology of the detected cells stained with Trypan blue, viable and dead cells could be differentiated (Fig. S2). The results from FIM were compared to the viability obtained from imaging flow cytometry (Fig. 1). In general, the viability of the freshly harvested Jurkat cells was higher in comparison to primary human T cells, which encountered a freeze-thaw and several purification steps. The viability of Jurkat cells with a mean of 86% was in good agreement for all three methods. In contrast, FIM showed slightly higher

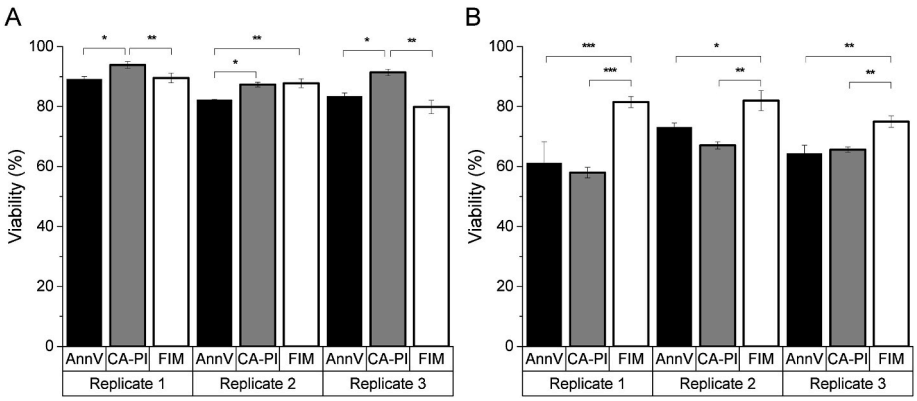

Fig. 1. Comparison of viability determined based on FIM and two different fluorescence assays. Viability of Jurkat cells (A) and T cells (B) derived from FIM images as well as determined by fluorescence assays Calcein AM & propidium iodide (CA-PI) and AnnexinV-FITC & PI (AnnV) for each measurement day. Duplicate measurements were performed for CA-PI and AnnV, whereas for FIM all viability data points generated for the osmotically inactive cell volume was taken into account (n = 5). *p < 0.05 was considered statistically significant, **p < 0.01 and ***p < 0.001 highly significant (one-way ANOVA).

viabilities of T cells of ca. 79% compared to imaging flow cytometry based on either AnnexinV-FITC/PI (66%) or Calcein AM/PI (64%) staining.

3.2. Osmotically inactive cell volume of Jurkat cells

The osmotically inactive cell volume V_b was determined for Jurkat cells based on FIM as well as Coulter counter by using the Boyle van't Hoff plot, which sets the cell volume in relation to the normalized osmolality. Fig. 2 shows the mean of three individual preparations (FIM) and three replicates (Coulter counter). The V_b value obtained from the y-intercept, which corresponds to the apparent cell volume at infinite osmolality, was calculated for each preparation (Table S7). Because of the morphological differentiation of the cells by FIM, V_b values for live as well as dead cells were obtained. In addition, both cell states were combined in order to mimic the situation of the Coulter counter. As expected, viable cells showed a strong change in cell volume when the tonicity of the medium was changed, which resulted in a low V_b of 49.3 ± 12.6%. In contrast, dead cells showed almost no osmotic response with a V_b of 84.6 ± 9.6%. Because of the overall high viability of the Jurkat cell preparation (see previous section), V_b of viable and dead cells combined of 53.8 ± 12.7% was only slightly higher than V_b of viable cells alone. Coulter counter measurements provided a V_b value of 65.5 ± 11% for the whole preparation because the measurement principle does not allow differentiation among viable and dead cells or debris particles. Moreover, FIM allowed exclusion of debris particle of similar size from the analysis which is not possible with the Coulter counter.

3.3. Membrane permeability of Jurkat cells towards water and CPA over time

Cell volume changes within the first 5 min upon addition of cells into CPA solutions were measured with FIM as well as Coulter counter at different temperatures. Fig. 3 shows an example of the kinetics of the cell volume response of Jurkat cells after exposure to 1.4 M Me_2SO at 22 °C. A huge variability in cell volumes were obtained but best-fit model and smoothed data were in good agreement for both methods. The mean cell volume decreases between start and the fastest possible measurement 8 s after addition of cells to sucrose solution (Fig. 4A and D) until the cell volume reaches an equilibrium value over time. L_p was determined based on cell volume shrinkage in the presence and absence of CPA. Upon exposure to permeable CPAs Me_2SO and glycerol Jurkat cells initially shrink and then swell back to their original volume (Fig. 4B–C and E–F). In addition, CPA permeability values (P_s) were calculated. Table 2 shows an overview of determined L_p and P_s values for Jurkat cells. As expected, L_p and P_s decreased at lower temperatures. However, L_p obtained for 30 °C was lower than expected as the value was decreasing compared to 20 °C. Water permeability in the presence of

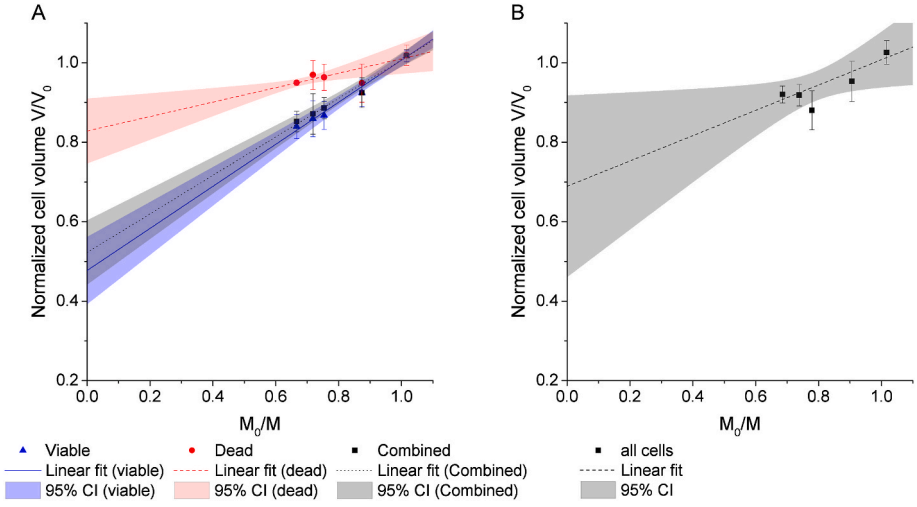

Fig. 2. Determination of osmotically inactive cell volume V_b for Jurkat cells based on FIM (A) and Coulter counter (B). Shown is the mean of three replicates and error bars represent the standard deviation. CI, confidence interval.

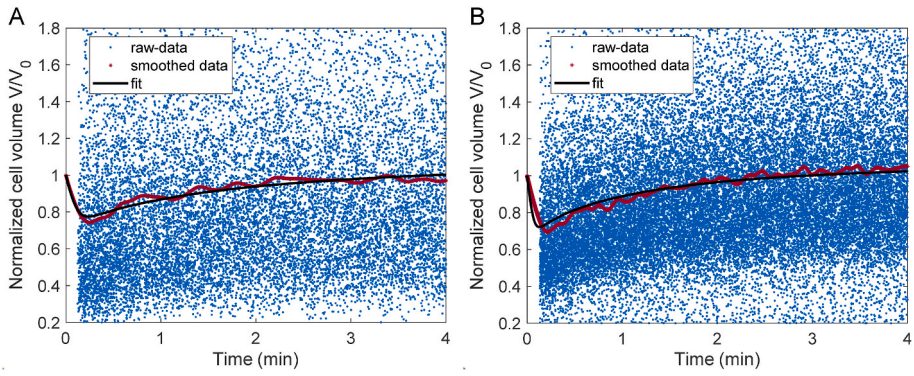

Fig. 3. Cell volume response of Jurkat cells during exposure to 1.4 M Me_2SO at 22 °C measured with FIM (A) and Coulter Counter (B). Blue symbols show individual cell volume measurements and the red line gaussian smoothed data points. The black line shows best-fit model predictions.

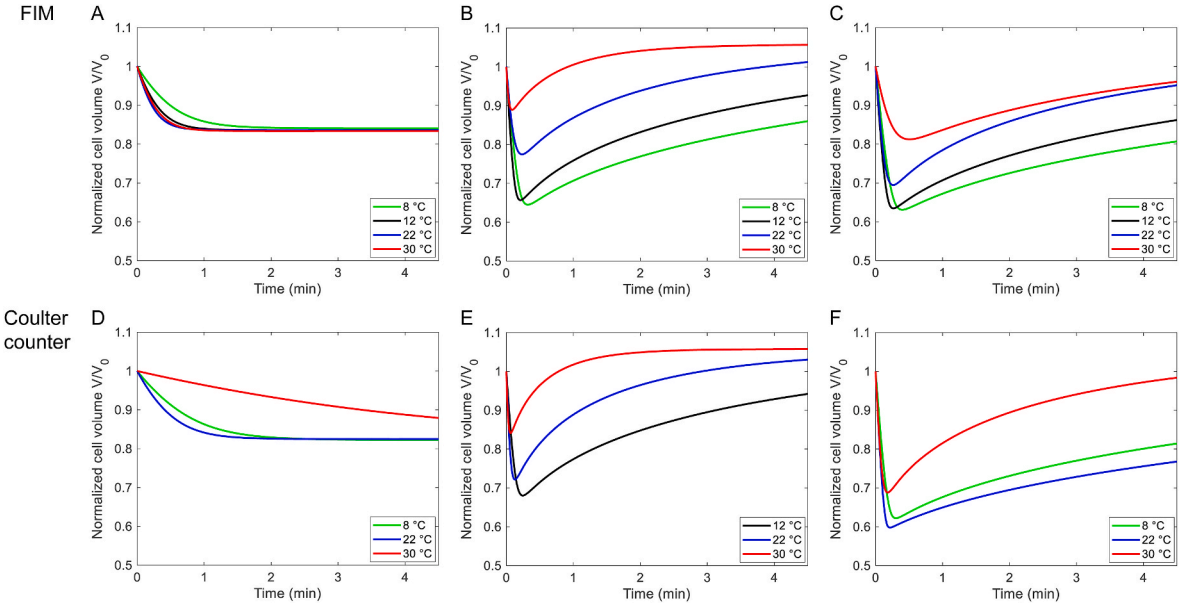

Fig. 4. Cell volume response of Jurkat cells during exposure to CPAs. Panels A–C show the osmotic response upon addition to sucrose in PBS (450 mOsm kg^{-1}) (A), 1.4 M Me_2SO in PBS (B) and 1.4 M glycerol in PBS (C) determined by FIM at four different temperatures. Panels D–F show the osmotic response upon exposure to sucrose in PBS (450 mOsm kg^{-1}) (D), 1.4 M Me_2SO in PBS (E) and 1.4 M glycerol in PBS measured by Coulter counter at three different temperatures. Best fit of approximately 20,000 and 35,000 data points are shown for FIM and Coulter counter, respectively.

permeating CPA, i.e., Me_2SO or glycerol, was lower compared to L_p determined for Jurkat cells upon exposure to sucrose in PBS. In general, glycerol showed a significant slower permeation for all temperatures except 8 °C in comparison to Me_2SO. The overall trends for L_p and P_s obtained with FIM and Coulter counter were similar. Nevertheless, differences in L_p upon exposure in sucrose in PBS were not as pronounced for the different temperatures for Coulter counter in comparison to FIM. Especially, L_p determined by Coulter counter at 30 °C was lower compared to FIM (Fig. 4D). L_p values obtained by Coulter counter in the presence of Me_2SO showed a higher increase with increasing temperatures in comparison to FIM. Glycerol permeability obtained by Coulter counter at room temperature was lower than expected because an increase in glycerol permeation at higher temperatures was observed for FIM.

3.4. Osmotic behavior of primary T cells determined by FIM

FIM experiments at room temperature were also performed with primary human T cells. V_b of T cells were measured by FIM based on three individual preparations (Fig. 5). For viable cells V_b was determined to be 47.8 ± 3.1%, which is comparable to V_b for viable Jurkat cells. Dead cells showed a higher V_b of 74.8 ± 3.6% increasing the value of the combined cell population to 53.8 ± 4.0%. Additionally, membrane permeability of T cells was measured at 22 °C by FIM upon addition of 150 mM sucrose in PBS (450 mOsm kg^{-1}), 1.4 M Me_2SO in PBS as well as 1.4 M glycerol in PBS as illustrated in Fig. 6. Calculated membrane permeabilities of T cells are shown in Table 3. Upon exposure to sucrose, water is moving out of the cells reaching their equilibrium volume after approximately 30 s. In comparison to Me_2SO glycerol is permeating significantly ($p < 0.05$) slower into the cell resulting in a lower P_s of 1.17 ± 0.154 μm min^{-1}. The P_s values of Me_2SO of Jurkat cells and T cells obtained by FIM were comparable, whereas P_s of glycerol for T cells was significantly lower ($p = 0.01$). However, L_p for primary T cells was determined to be approximately 3-fold lower in the presence of Me_2SO and glycerol compared to the values obtained for Jurkat cells (Table 3). Moreover, L_p in the presence of sucrose is an order of magnitude higher compared to that in the presence of glycerol or Me_2SO, which indicates that CPAs influence the membrane permeability towards water.

Table 2
Membrane permeability of Jurkat cells towards water and CPAs at different temperatures. –, not measured; n.a., not applicable because sucrose is an impermeable CPA.

CPA	Temp. [°C]	FIM		Coulter counter	
		L_p [µm min^{-1} atm^{-1}]	P_s [µm min^{-1}]	L_p [µm min^{-1} atm^{-1}]	P_s [µm min^{-1}]
Sucrose	8	0.201 ± 0.034	n.a.	0.116 ± 0.013	n.a.
	12	0.527 ± 0.245	n.a.	–	n.a.
	20	0.479 ± 0.091	n.a.	0.244 ± 0.028	n.a.
	30	0.264 ± 0.073	n.a.	0.142 ± 0.014	n.a.
Me_2SO	8	0.136 ± 0.006	0.606 ± 0.102	–	–
	12	0.192 ± 0.025	1.37 ± 0.309	0.144 ± 0.005	1.09 ± 0.079
	20	0.143 ± 0.034	3.90 ± 1.20	0.224 ± 0.025	3.13 ± 0.362
	30	0.320 ± 0.058	20.42 ± 2.50	0.468 ± 0.119	25.3 ± 7.20
Glycerol	8	0.127 ± 0.015	0.444 ± 0.062	0.103 ± 0.019	0.273 ± 0.079
	12	0.141 ± 0.021	0.616 ± 0.089	–	–
	20	0.151 ± 0.009	1.80 ± 0.182	0.175 ± 0.004	0.242 ± 0.011
	30[a]	0.060 ± 0.005	2.66 ± 0.500	0.157 ± 0.022	1.55 ± 0.241

[a] Based on duplicate measurement.

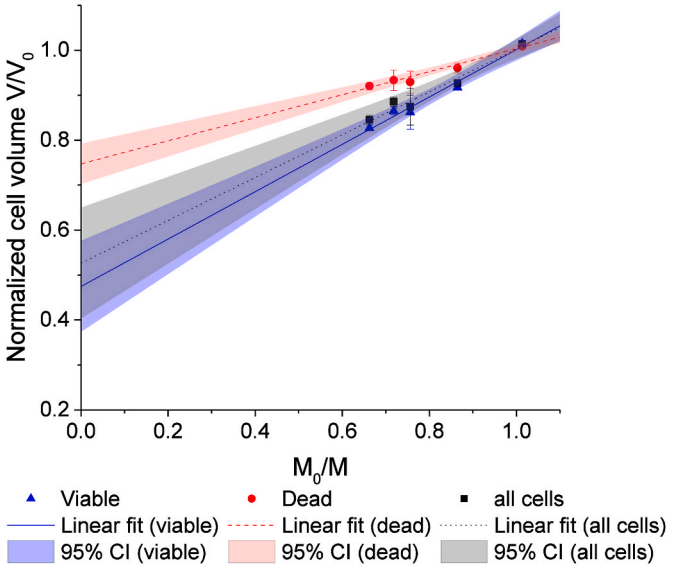

Fig. 5. Determination of osmotically inactive cell volume V_b for T cells based on Boyle van't Hoff plot by FIM. Shown is the mean of three replicates and error bars represent the standard deviation. CI, confidence interval.

3.5. Temperature dependence of membrane permeability of Jurkat cells

To determine the temperature dependence of membrane permeability of Jurkat cells towards water (L_p) in the absence of CPA, Arrhenius plots for both FIM and Coulter counter were generated as shown in Fig. 7. Additionally, the temperature dependence of L_p with CPA present and P_s were determined based on FIM (Fig. 8) and Coulter Counter (Fig. 9). Table 4 shows an overview of the resulting activation energies. Arrhenius plots for P_s resulted in a relatively good linear fit for both methods, whereas L_p showed a higher variation. Notably, the initial

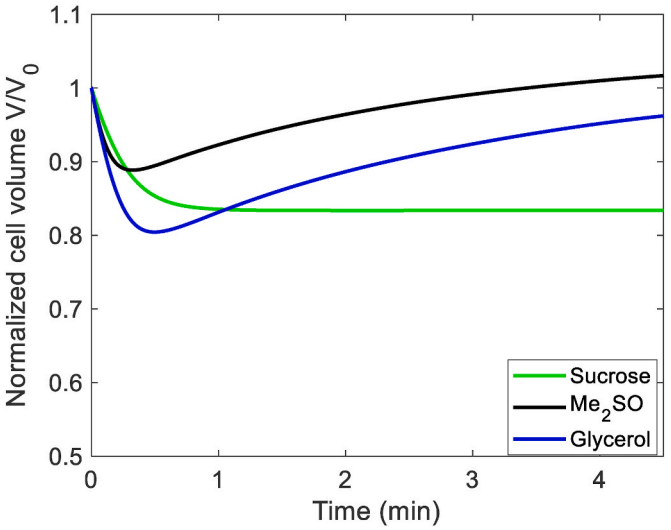

Fig. 6. Osmotic response upon addition of primary T cells towards Sucrose, Me_2SO and Glycerol determined at 22 °C by FIM.

Table 3
T cell membrane permeability at 22 °C calculated from FIM data. n.a., not applicable because sucrose is an impermeable CPA.

CPA	L_p [µm min^{-1} atm^{-1}]	P_s [µm min^{-1}]
Sucrose	0.345 ± 0.094	n.a.
Me_2SO	0.051 ± 0.017	3.30 ± 0.568
Glycerol	0.041 ± 0.002	1.17 ± 0.154

volume response cannot be measured within the first 8–10 s due to method limitations, which is particularly impacting the determined L_p at higher temperatures, when the response is faster. This can be seen from lower response values, which reduce the slope and consequently lead to apparently lower activation energies. For instance, activation energies for L_p without CPA of 1.5 kcal mol^{-1} were measured with both FIM and Coulter counter. Excluding the highest temperature L_p value changes E_{Lp} from 1.5 kcal mol^{-1} to 10–11 kcal mol^{-1} for FIM and Coulter counter. Nevertheless, slightly lower values for E_{Lp} were obtained in the presence of Me_2SO with Coulter counter and a 2-fold reduction was observed with FIM. Also, glycerol reduced E_{Lp} to 2.1 kcal mol^{-1} obtained for FIM and to 3.9 kcal mol^{-1} determined with Coulter counter. The activation energies for CPA permeabilities of Me_2SO and glycerol were in good agreement for both methods. The obtained activation energies of Me_2SO were approximately twice as high in comparison to glycerol for both methods.

4. Discussion

During cryopreservation intracellular ice formation as well as high solute concentration, known as the "two factor hypothesis" developed by Mazur et al. [18], are the two main factors influencing the success of a cryopreservation process of cells. In general, an intermediate freezing rate has to be chosen to enable sufficient dehydration of the cell to avoid intracellular ice formation as well as limit the stress due to increasing solute concentration during slow freezing [4,18]. To develop cell-specific cryopreservation processes biophysical characteristics such as V_b, L_p and P_s need to be determined [8]. Based on these parameters freezing protocols can be rationally developed ensuring sufficient CPA permeation while keeping the cells within their osmotic tolerance limits [12]. After CPA loading, the optimal cooling rate for cryopreservation can be predicted if L_p and its corresponding activation, E_{Lp} at subzero temperatures are known [29]. Generally, CPAs with a high P_s are favorable for cryopreservation as the equilibration time prior freezing can be minimized. Nevertheless, current methods to measure

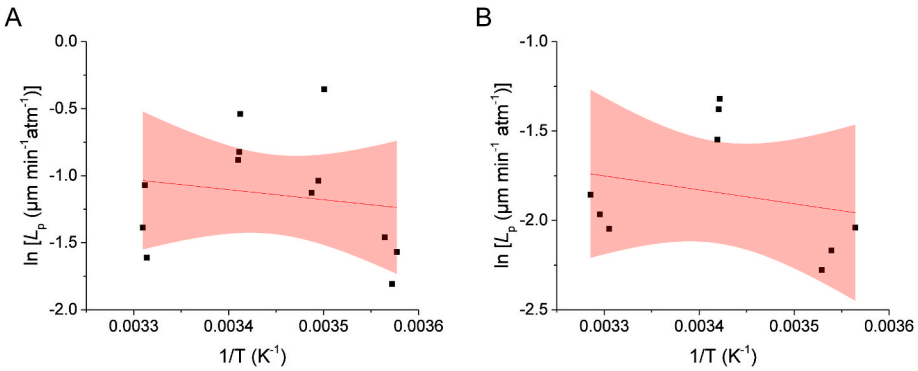

Fig. 7. Arrhenius plot of the water permeability L_p upon addition of Jurkat cells to sucrose in PBS (450 mOsm kg^{-1}) determined by FIM (A) and Coulter counter (B). Confidence interval 95%.

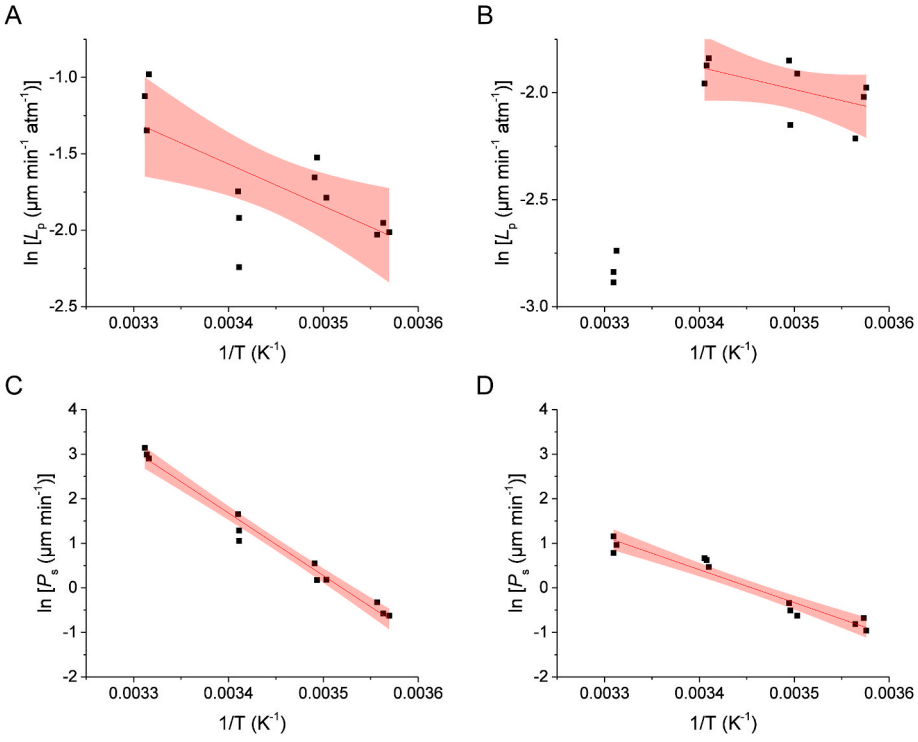

Fig. 8. Arrhenius plot of the water permeability L_p and CPA permeability P_s upon exposure of Jurkat cells to 1.4 M Me_2SO (A, C) and 1.4 M Glycerol (B, D) determined by FIM. Confidence interval 95%.

permeability parameters suffer from the inability to discriminate between viable and dead cells (Coulter counter) and the limited number of analyzed cells (microscopic set-ups). FIM already demonstrated its capabilities to discriminate cells from other particulate impurities. For instance, Vollrath et al. used FIM to differentiate cells from cell debris, silicone oil, glass particles and rubber stopper particles [28]. Furthermore, Dynabeads, a common particulate reagent to activate T cells in the process of CAR T cell production could be identified and discriminated from Jurkat cells using machine learning [10]. Furthermore, machine learning allowed to determine the viability of Jurkat cells using FIM in previous work [9].

In this study, we stained dead cells by using Trypan blue which allowed the differentiation of viable and dead cells with traditional morphological filters from the FIM software. The FIM-based method was well in line with the fluorescence-based viability methods using imaging flow cytometry. However, as T cells are smaller in comparison to Jurkat cells, it is more challenging to differentiate cell debris and dead cells and a stricter lower diameter filter was used to exclude debris particles with FIM. This might have impacted the viability determination of T cells resulting in a slightly higher (10–15%) apparent viability obtained with FIM as compared to fluorescence.

Whereas Coulter counter cannot differentiate between viable and dead cells as well as debris, the morphological differentiation by FIM allowed to measure the osmotic response of the subpopulations. As expected, dead cells showed no osmotic response [19], which increases the average V_b of all cells (53.8%) compared to the subpopulation of only viable cells (49.3 ± 12.6%). Comparable V_b values of Jurkat cells over a broad range are reported in literature: 48.0% [22], 49.6% [30], 53.1% [25] and 67.4% [8]. Possibly, differences in the obtained V_b values could result from the fact that the methods used in mentioned studies could not discriminate cell condition and thus the viability of the preparation directly impacted the measured V_b values. The resulting V_b determined by Coulter counter for the whole population of Jurkat cells (incl. dead cells) was 65.3 ± 12%, which is at the upper end of reported literature values. Thus, possibly overestimating the osmotically inactive cell volume, which can lead to inaccurately designed cryopreservation

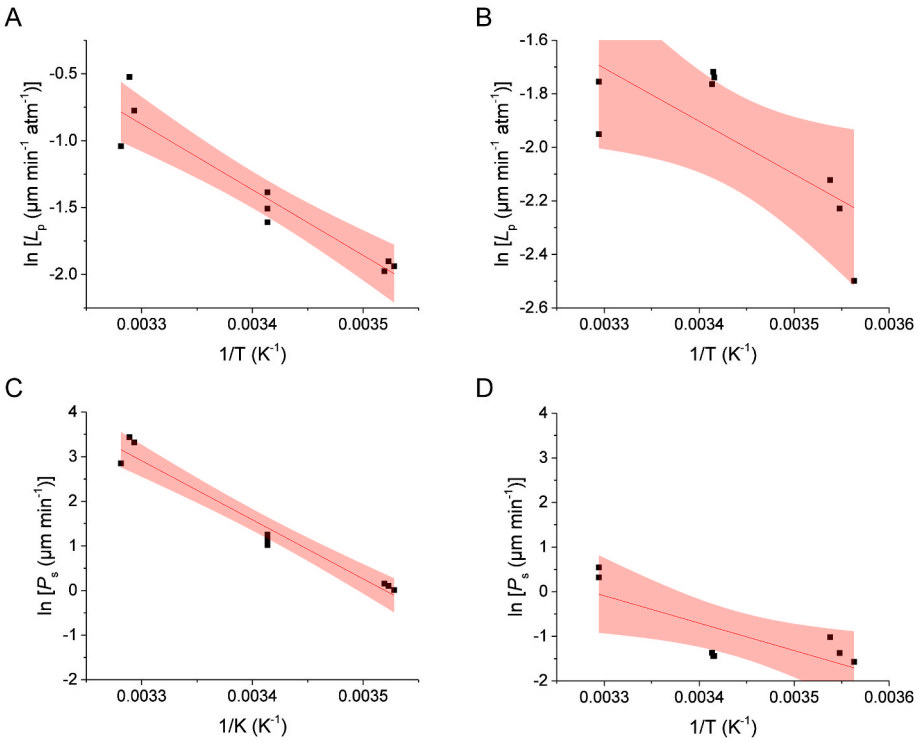

Fig. 9. Arrhenius plot of the water permeability L_p and CPA permeability P_s upon exposure of Jurkat cells to 1.4 M Me_2SO (A, C) and 1.4 M Glycerol (B, D) determined by Coulter counter. Confidence interval 95%.

Table 4
Activation energies of membrane permeabilities determined by FIM and Coulter counter for Jurkat cells. n.a., not applicable because sucrose is an impermeable CPA.

CPA	FIM		Coulter counter	
	E_{Lp} [kcal mol^{-1}]	E_{Ps} [kcal mol^{-1}]	E_{Lp} [kcal mol^{-1}]	E_{Ps} [kcal mol^{-1}]
Sucrose	1.5 ± 2.7	n.a.	1.6 ± 2.3	n.a.
Me_2SO	5.5 ± 1.8	27.9 ± 1.3	9.7 ± 1.2	26.3 ± 2.1
Glycerol	2.1[a] ± 1.2	14.7 ± 1.2	3.9 ± 1.5	12.2 ± 4.1

[a] Based on 8 °C, 12 °C and 20 °C.

procedures [21]. Thus, a CPA loading and unloading regime based on the more correct V_b of viable Jurkat cells is warranted. Interestingly, the obtained V_b of viable primary T cells was 47.8 ± 3.1%, which is comparable to the value for viable Jurkat cells indicating that they may be a good model cell line for primary human T cells to establish cryopreservation protocols. Slower permeabilities of water and CPAs could be observed by both FIM and Coulter counter measurements. Moreover, at room temperature, Me_2SO is permeating faster into the cell in comparison to glycerol for both Jurkat and primary T cells. For Jurkat cells this trend was also shown at temperatures 8, 12 and 30 °C. The obtained permeabilities for Jurkat and primary T cells L_p in the presence of sucrose in PBS as well as L_p and P_s in the presence of Me_2SO in PBS was in range with reported literature values (Table 5). However, the values vary between applied techniques, and also different media were reported in the literature (PBS or 0.9% sodium chloride solutions). For both Jurkat as well as primary T cells L_p in the presence of permeable CPA is reduced compared to L_p without permeable CPA indicating an influence of CPA on the transport of water. A reduction of L_p in the presence of permeable CPA has been previously reported [8,23,25], although the mechanism of action is currently unknown. The slower permeation of glycerol in comparison to Me_2SO results in a higher cell

Table 5
Comparison of L_P and P_S of different cell types.

Cell line	Temp. [°C]	CPA	L_p [µm min^{-1} atm^{-1}]	P_s [µm min^{-1}]	Technique	Ref.
Jurkat cells	20	1.4 M Me_2SO in PBS	0.143 ± 0.034	3.90 ± 1.20	FIM	Current study
Jurkat cells	20	1.4 M Glycerol in PBS	0.151 ± 0.009	1.80 ± 0.182	FIM	Current study
Jurkat cells	22	10% (v/v) Me_2SO in PBS	0.158 ± 0.011	0.42 ± 0.04	Microfluidic device	[8]
Jurkat cells	22	10% (v/v) Me_2SO in PBS	0.148 ± 0.051	3.4 ± 1.4	Microfluidic device	[30]
Jurkat cells	22	10% (v/v) Me_2SO in 0.9% NaCl	0.1564 ± 0.0018	5.453 ± 0.054	Micro-vortex System (Microfluidic based)	[25]
Granulocytes	21	10% (v/v) Me_2SO in DPBS	0.21	6.4	Coulter Counter	[27]
Granulocytes	21	0.7 mOsm kg^{-1} Glycerol in DPBS	0.18	1.0	Coulter Counter	[27]
Human vaginal mucosal T cells	Room temp.	10% (v/v) Me_2SO in 0.9% NaCl	0.089 ± 0.051	4.72 ± 2.30	Microfluidic perfusion system	[23]
Human vaginal mucosal T cells	Room temp.	1.5 M Glycerol in 0.9% NaCl	0.055 ± 0.003	0.05 ± 0.04	Microfluidic perfusion system	[23]

volume excursion, which might impact the cell viability [23]. In general, CPA permeation of primary T cells and Jurkat cells showed a similar osmotic response upon exposure to CPA solutions at room temperature. Therefore, also the CPA equilibration process and freezing rate for T cells could be derived from L_p and P_s values of Jurkat cells.

Additionally, the activation energy for L_p and P_s was determined for Jurkat cells based on FIM and Coulter counter measurements. The resulting activation energy for L_p of 10–11 kcal mol^{-1} excluding the value at 30 °C is in range with reported literature values of 7.075 kcal mol^{-1} [8] and 11.36 kcal mol^{-1} [25]. In general, lower activation energies for water permeability were calculated in the presence of CPA, with values obtained by FIM being even lower in comparison to Coulter counter values. In literature different trends were reported. Tseng et al. observed an E_{Lp} of 11.36 kcal mol^{-1} for a binary system, which slightly decreased to 10.87 kcal mol^{-1} in presence of Me_2SO [25]. In contrast, Fang et al. reported an increase of the water permeability activation energy in the presence of Me_2SO from 7.075 kcal mol^{-1} to 9.566 kcal mol^{-1} [8].

A good correlation between the activation energies for P_s of Me_2SO obtained for FIM and Coulter counter was observed with E_{Ps} of 27.9 and 26.3 kcal mol^{-1}, respectively. Both values were in the range of literature values with E_{Ps} of 34.416 kcal mol^{-1} [8] and 18.64 kcal mol $^{-1}$ for Me_2SO [25]. Furthermore, activation energy for glycerol was comparable to reported activation energies for granulocytes with 16.24 kcal mol^{-1} [27] and for spermatozoa with 11.6 kcal mol^{-1} [6]. Having a higher activation energy, membrane permeability towards Me_2SO is influenced more by changes in temperature in comparison to glycerol, possibly making it a more suitable CPA for Jurkat cells as equilibration times during CPA addition at slightly higher temperatures can be shortened [8]. Within this study a faster permeation of Me_2SO into Jurkat and primary T cells was observed compared to glycerol, confirming that Me_2SO is a more suitable CPA for these cell types.

Nevertheless, FIM as well as Coulter counter techniques have their advantages and disadvantages. Both methods measure cell volume after a time lag of several seconds, which possibly has an impact on measuring the cell volume decrease. Therefore, L_p was difficult to determine especially at higher temperatures as water is moving out of the cells within the first 30 s. Overall obtained osmotic values for FIM and Coulter counter showed similar trends, although some experiments resulted in different values such as with samples containing glycerol, which can possibly be attributed to the different measurement principles. In FIM cell size is based on bright-field images after selection of viable, Trypan blue-stained cells whereas in Coulter counter a change in electrical resistance is correlated with cell size. The Coulter counter instrument has to be calibrated for each used solution and differences in the ionic strength and temperature deviations can lead to different sizing results [15]. As V_0 and time measurements are in different solutions, the sizing can be influenced. For both methods a high variation of measured cell size was observed as shown in Fig. 3, which has been also observed previously [5,27]. Additionally, it is noticeable, that the number of analyzed cells within a Coulter counter measurement are approximately 1.5 times higher than for FIM, which can be also seen in Fig. 3. For FIM a differentiation between viable and dead cells was done based on Trypan blue staining, whereas in Coulter counter experiments all cells within a specific size range were used to determine osmotic behaviors. Furthermore, the field of view within the microscopic set-up of the FIM is relatively narrow leading to approximately 25% unfocused images within one measurement which have to be excluded from the analysis by morphological parameters.

5. Conclusion

In this study, a new method based on FIM was developed to determine the osmotic response of cells upon exposure to CPA solutions. These results were in good agreement with results obtained from Coulter counter measurements, a standard method for this purpose, as well as reported literature values. Within FIM Trypan blue staining was used, which allows for viability determination using morphological filters. Therefore, FIM method provides further insights into the osmotic behavior of different subpopulations of cells. The osmotic response of Jurkat cells and primary human T cells upon exposure to osmotic solutions at room temperature were comparable showing that Jurkat cells are potentially a good model for (CAR) T cells to develop cryopreservation processes. Osmotically inactive cell volume of viable cells was determined enabling a more accurate prediction of volume excursions within the tolerance limit of the cell during CPA loading.

Author contributions (CRediT)

AR: Conceptualization, Investigation, Data Curation, Visualization, Writing – Original Draft. RW: Investigation, Resources. CW: Resources. WW: Conceptualization, Resources. GK: Conceptualization, Writing – Review & Editing Supervision. TM: Conceptualization, Writing – Review & Editing, Supervision.

Declaration of competing interest

The authors declare that they have no known competing financial interests or personal relationships that could have appeared to influence the work reported in this paper.

Acknowledgements

WW was financially supported via grant WO1735/6-2 of the German Research Foundation (DFG: Deutsche Forschungsgemeinschaft). We sincerely acknowledge Wim Jiskoot (1961–2021), who initiated this project and was involved in the initial discussions.

Appendix A. Supplementary data

Supplementary data to this article can be found online at https://doi.org/10.1016/j.cryobiol.2023.104587.

References

[1] A.B. Araújo, G.D. Salton, M.H. Angeli, J.M. Furlan, T. Schmalfuss, L.M. Röhsig, Effects of cell concentration, time of fresh storage, and cryopreservation on peripheral blood stem cells: PBSC fresh storage and cryopreservation, Transfus. Apher. Sci. 61 (2022), 103298. https://10.1016/j.transci.2021.103298.
[2] A. Bak, K.P. Friis, Y. Wu, R.J.Y. Ho, Translating cell and gene biopharmaceutical products for health and market impact. Product scaling from clinical to marketplace: lessons learned and future outlook, J. Pharmaceut. Sci. 108 (2019) 3169–3175. https://10.1016/j.xphs.2019.05.027.
[3] J.G. Baust, D. Gao, J.M. Baust, Cryopreservation: an emerging paradigm change, Organogenesis 5 (2009) 90–96. https://10.4161/org.5.3.10021.
[4] J.M. Baust, L.H. Campbell, J.W. Harbell, Best practices for cryopreserving, thawing, recovering, and assessing cells, in vitro cell, Dev. Biol. Anim 53 (2017) 855–871. https://10.1007/s11626-017-0201-y.
[5] E. Casula, G.P. Asuni, V. Sogos, S. Fadda, F. Delogu, A. Cincotti, Osmotic behaviour of human mesenchymal stem cells: implications for cryopreservation, PLoS One 12 (2017), e0184180. https://10.1371/journal.pone.0184180.
[6] J. Du, F.W. Kleinhans, P. Mazur, J.K. Critser, Human spermatozoa glycerol permeability and activation energy determined by electron paramagnetic resonance, Biochim. Biophys. Acta 1194 (1994) 1–11. https://10.1016/0005-2736(94)90196-1.
[7] G.D. Elliott, S. Wang, B.J. Fuller, Cryoprotectants: a review of the actions and applications of cryoprotective solutes that modulate cell recovery from ultra-low temperatures, Cryobiology 76 (2017) 74–91. https://10.1016/j.cryobiol.2017.04.004.
[8] C. Fang, F. Ji, Z. Shu, D. Gao, Determination of the temperature-dependent cell membrane permeabilities using microfluidics with integrated flow and temperature control, Lab. Chip 17 (2017) 951–960. https://10.1039/c6lc01523a.
[9] A.D. Grabarek, W. Jiskoot, A. Hawe, K. Pike-Overzet, T. Menzen, Forced degradation of cell-based medicinal products guided by flow imaging microscopy: explorative studies with Jurkat cells, Eur. J. Pharm. Biopharm. 167 (2021) 38–47. https://10.1016/j.ejpb.2021.07.004.
[10] A.D. Grabarek, E. Senel, T. Menzen, K.H. Hoogendoorn, K. Pike-Overzet, A. Hawe, W. Jiskoot, Particulate impurities in cell-based medicinal products traced by flow imaging microscopy combined with deep learning for image analysis, Cytotherapy 23 (2021) 339–347. https://10.1016/j.jcyt.2020.04.093.

[11] K.H. Hoogendoorn, D.J.A. Crommelin, W. Jiskoot, Formulation of cell-based medicinal products: a question of life or death? J. Pharmaceut. Sci. 110 (2021) 1885–1894. https://10.1016/j.xphs.2020.07.002.
[12] J.D. Benson, Mathematical modeling and optimization of cryopreservation in single cells, in: W.F. Wolkers, H. Oldenhof (Eds.), Cryopreservation and Freeze-Drying Protocols, Springer US, New York, NY, 2021, pp. 129–172.
[13] G.S. Kao, H.T. Kim, H. Daley, J. Ritz, S.R. Burger, L. Kelley, C. Vierra-Green, S. Flesch, S. Spellman, J. Miller, D. Confer, Validation of short-term handling and storage conditions for marrow and peripheral blood stem cell products, Transfusion 51 (2011) 137–147. https://10.1111/j.1537-2995.2010.02758.x.
[14] F.W. Kleinhans, Membrane permeability modeling: Kedem-Katchalsky vs a two-parameter formalism, Cryobiology 37 (1998) 271–289. https://10.1006/cryo.1998.2135.
[15] R.W. Lines, The electrical sensing zone method (the Coulter principle), in: Stanley-Wood, Lines (Ed.), Particle Size Analysis, 1992, pp. 350–373.
[16] J. Lotz, S. Içli, D. Liu, S. Caliskan, H. Sieme, W.F. Wolkers, H. Oldenhof, Transport processes in equine oocytes and ovarian tissue during loading with cryoprotective solutions, Biochim. Biophys. Acta Gen. Subj. 1865 (2021), 129797. https://10.1016/j.bbagen.2020.129797.
[17] J.B. Mandumpal, C.A. Kreck, R.L. Mancera, A molecular mechanism of solvent cryoprotection in aqueous DMSO solutions, Phys. Chem. Chem. Phys. 13 (2011) 3839–3842. https://10.1039/c0cp02326d.
[18] P. Mazur, S.P. Leibo, E.H.Y. Chu, A two-factor hypothesis of freezing injury, Exp. Cell Res. 71 (1972) 345–355. https://10.1016/0014-4827(72)90303-5.
[19] H. Oldenhof, A.-K. Blässe, W.F. Wolkers, H. Bollwein, H. Sieme, Osmotic properties of stallion sperm subpopulations determined by simultaneous assessment of cell volume and viability, Theriogenology 76 (2011) 386–391. https://10.1016/j.theriogenology.2011.02.027.
[20] C.-H. Pi, G. Yu, P.I. Dosa, A. Hubel, Characterizing modes of action and interaction for multicomponent osmolyte solutions on Jurkat cells, Biotechnol. Bioeng. 116 (2019) 631–643. https://10.1002/bit.26880.
[21] R. Raju, S.J. Bryant, B.L. Wilkinson, G. Bryant, The need for novel cryoprotectants and cryopreservation protocols: insights into the importance of biophysical investigation and cell permeability, Biochim. Biophys. Acta Gen. Subj. 1865 (2020), 129749. https://10.1016/j.bbagen.2020.129749.
[22] R. Reuss, J. Ludwig, R. Shirakashi, F. Ehrhart, H. Zimmermann, S. Schneider, M. M. Weber, U. Zimmermann, H. Schneider, V.L. Sukhorukov, Intracellular delivery of carbohydrates into mammalian cells through swelling-activated pathways, J. Membr. Biol. 200 (2004) 67–81. https://10.1007/s00232-004-0694-7.
[23] Z. Shu, S.M. Hughes, C. Fang, J. Huang, B. Fu, G. Zhao, M. Fialkow, G. Lentz, F. Hladik, D. Gao, A study of the osmotic characteristics, water permeability, and cryoprotectant permeability of human vaginal immune cells, Cryobiology 72 (2016) 93–99. https://10.1016/j.cryobiol.2016.03.003.
[24] B. Sydykov, H. Oldenhof, H. Sieme, W.F. Wolkers, Storage stability of liposomes stored at elevated subzero temperatures in DMSO/sucrose mixtures, PLoS One 13 (2018), e0199867. https://10.1371/journal.pone.0199867.
[25] H.-Y. Tseng, C.-J. Chen, Z.-L. Wu, Y.-M. Ye, G.-Z. Huang, The non-contact-based determination of the membrane permeability to water and dimethyl sulfoxide of cells virtually trapped in a self-induced micro-vortex, Lab Chip 22 (2022) 354–366. https://10.1039/d1lc00846c.
[26] S. Upadhaya, J.X. Yu, M. Shah, D. Correa, T. Partridge, J. Campbell, The clinical pipeline for cancer cell therapies, Nat. Rev. Drug Discov. 20 (2021) 503–504. https://10.1038/d41573-021-00100-z.
[27] A.M. Vian, A.Z. Higgins, Membrane permeability of the human granulocyte to water, dimethyl sulfoxide, glycerol, propylene glycol and ethylene glycol, Cryobiology 68 (2014) 35–42. https://10.1016/j.cryobiol.2013.11.004.
[28] I. Vollrath, R. Mathaes, A.S. Sediq, D. Jere, S. Jörg, J. Huwyler, H.-C. Mahler, Subvisible particulate contamination in cell therapy products-can we distinguish? J. Pharmaceut. Sci. 109 (2020) 216–219. https://10.1016/j.xphs.2019.09.002.
[29] W.F. Wolkers, H. Oldenhof, Principles underlying cryopreservation and freeze-drying of cells and tissues, in: W.F. Wolkers, H. Oldenhof (Eds.), Cryopreservation and Freeze-Drying Protocols, Springer US, New York, NY, 2021, pp. 3–25.
[30] T. Yang, J. Peng, Z. Shu, P.K. Sekar, S. Li, D. Gao, Determination of the membrane transport properties of Jurkat cells with a microfluidic device, Micromachines 10 (2019) 832. https://10.3390/mi10120832.
[31] S. Zölls, R. Tantipolphan, M. Wiggenhorn, G. Winter, W. Jiskoot, W. Friess, A. Hawe, Particles in therapeutic protein formulations, Part 1: overview of analytical methods, J. Pharmaceut. Sci. 101 (2012) 914–935. https://10.1002/jps.23001.